Original Article

High resolution optical coherence elastography of retina under prosthetic electrode

Runze Li[1,2#], Zhaodong Du[2#], Xuejun Qian[1,2], Yan Li[3,4], Juan-Carlos Martinez-Camarillo[2], Laiming Jiang[2], Mark S. Humayun[1,2], Zhongping Chen[3,4], Qifa Zhou[1,2]

[1]Department of Biomedical Engineering, University of Southern California, Los Angeles, CA, USA; [2]USC Roski Eye Institute, University of Southern California, Los Angeles, CA, USA; [3]Beckman Laser Institute, University of California, Irvine, CA, USA; [4]Department of Biomedical Engineering, University of California, Irvine, CA, USA

[#]These authors contributed equally to this work.

Correspondence to: Zhongping Chen. University of California, 1002 Health Sciences Road East, Irvine, CA 92617, USA. Email: z2chen@uci.edu; Qifa Zhou. 1042 Downey Way, LA, CA 90089-1111, USA. Email: qifazhou@usc.edu.

Background: Quantitatively investigating the biomechanics of retina with a retinal prosthetic electrode, we explored the effects of the prosthetic electrode on the retina, and further supplemented data for a potential clinical trial.

Methods: Biomechanical properties were assessed with a high resolution optical coherence tomography (OCT) based elastography (OCE) system. A shaker was used to initiate elastic waves and an OCT system was used to track axial displacement along with wave propagation. Rabbits received surgery to implant the retinal prosthetic electrode, and elastic wave speed was measured before and after implantation; anatomical B-mode images were also acquired.

Results: Spatial-temporal maps of each layer in retina with and without prosthetic electrodes were acquired. Elastic wave speed of nerve fiber to inner plexiform layer, inner nuclear to outer nuclear layer, retinal pigmented epithelium layer and choroid to sclera layer without prosthetic electrode were found to be 3.66±0.36, 5.33±0.07, 6.85±0.37, and 9.69±0.24 m/s, respectively. With prosthetic electrode, the elastic wave speed was found to be 4.09±0.26, 5.14±0.11, 6.88±0.70, and 9.99±0.73 m/s, respectively in each layer.

Conclusions: Our results show that the elastic wave speed in each layer of retina is slightly faster with the retinal electrode, and further demonstrate that the retinal prosthetic electrode does not affect biomechanical properties significantly. In the future, we expect OCE technology to be used by clinicians where it could become part of routine testing and evaluation of the biomechanical properties of the retina in response to long term use of prosthetic electrodes in patients.

Keywords: Optical coherence elastography; elastic wave propagation; mechanical shaker; retinal prosthetic electrode

Submitted Oct 08, 2020. Accepted for publication Dec 15, 2020.
doi: 10.21037/qims-20-1137
View this article at: http://dx.doi.org/10.21037/qims-20-1137

Introduction

Diseases of the posterior segment of the eye, including age-related macular degeneration (AMD) and retinitis pigmentosa (RP), damage photoreceptors and their supporting epithelial cells (1). More than 1 million patients are affected by RP worldwide. Initially, patients retain their central visual field with gradual peripheral vision loss, however, eventually they will go on to lose both areas of vision with progression of the disease (2). AMD is the leading cause of blindness in patients aged 65 or older in

developed countries, with more than 8 million Americans suffering from the disease (3). Currently, there is no known cure to reverse the progressive loss of photoreceptors due to these two conditions.

Retinal prosthetic electrodes hold the potential to restore some visual functions by directly stimulating the neural retina with electrical pulses (4). The Argus® II retinal prosthetic electrode (SSMP, Sylmar, CA, USA) is the first and only commercial product that has received the European conformity mark and been approved by the U.S. Food and Drug Administration (FDA) (5). With Argus II, a camera mounted to a pair of glasses worn by the patient first captures the visual signals from the patient's environment and these are then sent to a video processing unit, through a transmitting coil. The received electrical signals are then used to drive corresponding in-eye mounted electrodes which then directly stimulate the patient's retina thereby creating the experience of vision where previously none existed (6). A flexible polyimide (PI) based microelectrode array stimulates the epiretinal side of the retina. The safety and bio-compatibility of PI electrodes has been previously investigated, however, the biomechanical effects of retinal prosthetic electrodes on the posterior segment of the eye still remain unknown (7-10).

Biomechanical properties of ocular tissues are crucial for the health of both the anterior and posterior segments of the eye, with many ocular diseases being associated with altered biomechanics. Keratoconus is a prevalent disease which leads to significant visual impairment due to the development of a cone-shaped ectatic cornea, and one of its clinical signs is an unusually compliant cornea compared with normal cornea (11). It has been shown that mechanical properties of the posterior segment of the eye change with progression of diseases such as glaucoma (12). The biomechanics of lamina cribrosa (LC) has been postulated to play a pivotal role in ganglion cell dystrophies in glaucoma (13,14). The retina also suffers mechanical alteration with progression of blood vessel infiltration due to AMD (15).

Elastography is a widely used imaging modality to reconstruct biomechanics in soft tissue in a non-invasive manner, and is often used to provide supplementary diagnoses for standard structural imaging. There are several methods available for measuring biomechanics by elastography, including conventional ultrasound elastography (16,17), high resolution ultrasound elastography (18-20) and optical coherence tomography (OCT) based elastography (OCE) (21,22). Among these techniques, OCE is the most promising imaging modality in the field of ophthalmology owing to the advantages of high resolution (<10 μm), high sensitivity, and the transparency of ocular tissue. OCE has been widely used in mapping the elasticity of ocular tissue, such as cornea (23), lens (24), retina (25), and optic nerve head (26).

To initiate the propagation of an elastic wave, several excitation methods have been employed, such as air-puff (27), acoustic micro-tapping (28), and acoustic radiation force (ARF) (23,26). Both air-puff and acoustic micro-tapping are capable of reconstructing biomechanical roperties of the anterior segment of the eye. However, due to the natural geometry of the eye and attenuation that occurs over the long distance from the anterior to the posterior segment, these methods are not optimal in this study. Qu *et al.* first utilized ARF-OCE to reconstruct the biomechanical properties in each layer of retina *in vivo* (23). To induce desirable tissue motion to track elastic waves, high power ARF is required. Due to strict FDA regulation in ophthalmic exposure to ultrasound, the mechanical index and acoustic intensity prevent this technology from being used in the clinic. Zhou *et al.* utilized a shaker to induce harmonic vibration, and an ultrasonic array to measure induced wave propagation in the posterior sclera in humans (17). Qian *et al.* applied a shaker as a vibrating source to induce tissue motion, and demonstrated feasibility for reconstruction of biomechanical properties of the retina in rabbit eye (25).

In this study, we propose to use a shaker-based OCE technology to evaluate biomechanical properties in the retina with prosthetic electrodes, potentially supplementing the data set used for evaluation of the Argus II retinal prosthetic electrode, and then translating this technology into clinical use.

Methods

Experimental setup

System settings have been shown elsewhere (25). Briefly, as shown in *Figure 1*, a spectral domain optical coherence tomography system (SD-OCT) with center wavelength of 890 nm and bandwidth of 144 nm was developed to image tissue structure as well as to track elastic wave propagation. A mechanical shaker (mini-shaker type 4810; Bruel & Kjaer, Duluth, Georgia, USA) was used to induce tissue motion and initiate elastic waves. The rod tip of the shaker was placed on the corneal limbus and aligned in the direction

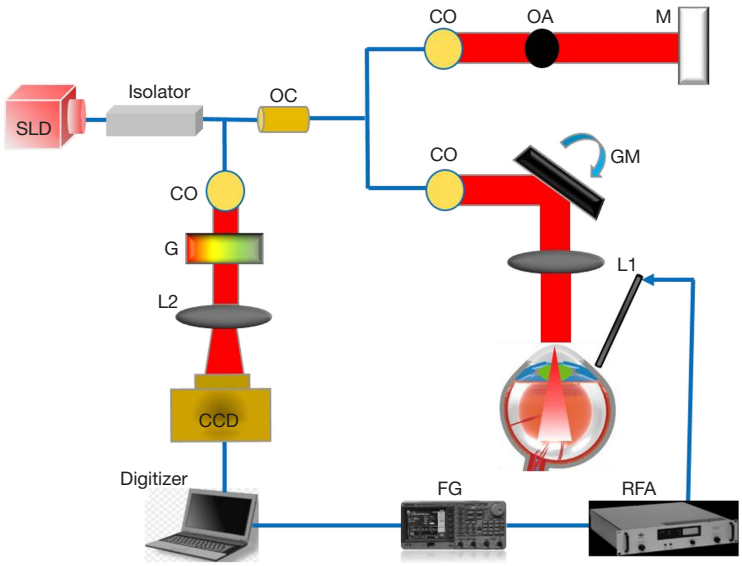

Figure 1 Schematic of shaker based OCE system. OCE, optical coherence tomography based elastography; SLD, superluminescent diode; OC, optical coupler; CO, collimator; OA, optical attenuator; M, mirror; GM, galvanometer mirrors; L1/L2, lens; RFA, radiofrequency amplifier; FG, function generator; G, grating.

of the OCT scanning beam with real time Doppler OCT imaging. A step size of 6 μm was used for the scanning galvanometer mirror positioning system (galvo) and a total of 500 positions were scanned.

To precisely induce and track elastic wave propagation, all components of the system were synchronized. A baseband signal generated by the personal computer (PC) triggered an arbitrary function generator (AFG 3252C, Tektronix, Beaverton, OR, USA). A 0.6 ms pulse-width impulse signal was used to generate detectable axial displacement with broad bandwidth (25). The impulse signal was amplified using a power amplifier (Type 2718, Bruel & Kjaer, Duluth, Georgia, USA) and finally transmitted to the shaker. A series of 400 A-lines was acquired at every position corresponding to 8.8 ms before the galvo translated to the next position. Inter-A-line analysis was performed with a 20 μs time interval to obtain axial displacements for further processing (24). Inter-A-line analysis was insensitive to motion artifacts because the data acquisition frequency was much faster than the motion frequency, and adequate anesthesia was administrated to reduce the motion artifact.

Post-processing and data analysis

After scanning in each lateral position, raw data was saved to disk for off-line processing. Depth-resolved OCT intensity data and phase-resolved Doppler OCT data were first obtained. To calculate the elastic wave speed, the spatial-temporal map was reconstructed at each lateral position and time. The elastic wave speed can be estimated with known propagation distance and time. To precisely calculate the wave speed, linear regression was used for all successive peak axial displacements at each lateral position in the corresponding spatial-temporal map. In this study, the elastic wave speed in each layer was measured before and after the implant of prosthetic electrode, the Shapiro-Wilk test was performed to evaluate the normality of the speed distribution, and the paired *t*-test was performed to evaluate the statistical significance.

Implant surgery

Surgery protocol was approved by the University of Southern California Institutional Animal Care and Use Committee (IACUC). Prior to surgery, Dutch Belted Pigmented rabbits (~2 kg) were anesthetized with ketamine (35 mg/kg) and xylazine (5 mg/kg) through subcutaneous injection. Additional anesthesia was induced using 2.5% sevoflurane through a facial mask. One drop of 0.5% proparacaine hydrochloride ophthalmic solution was administrated topically for ocular anesthesia, and 1 drop of 1% tropicamide and 2.5% phenylephrine was applied

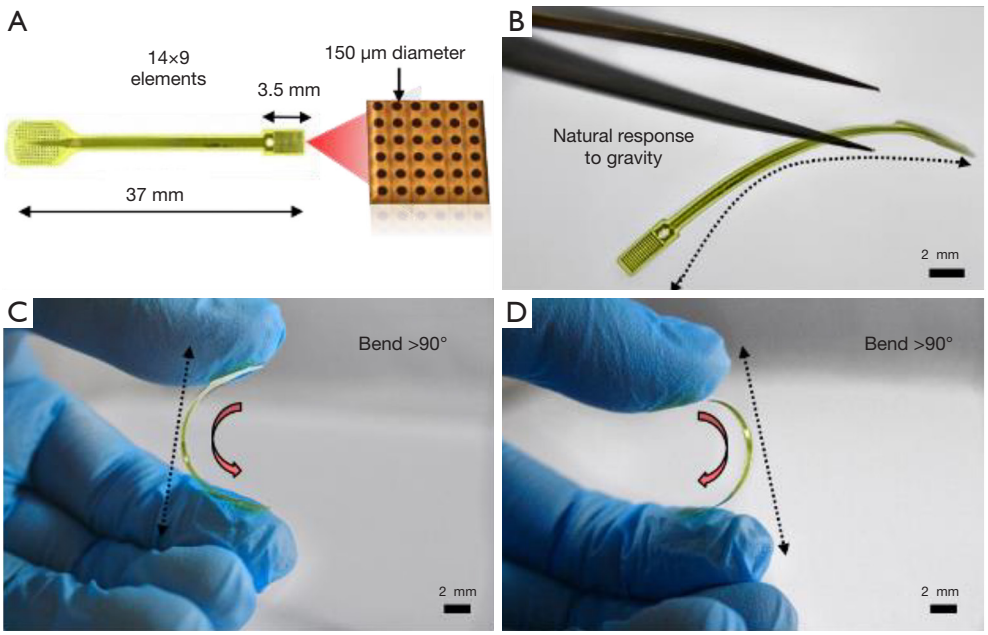

Figure 2 Characterizations of retinal prosthetic electrode. (A) Structural image of the prosthesis; (B,C,D) optical images of the flexible prosthesis when it stands freely, bends convexly and concavely with more than 90°.

in the same way for eye dilation. Heart-rate, respiration, oxygen saturation, body temperature, non-invasive blood pressure, oxygen flow and end tidal carbon dioxide (when sevoflurane was used), were recorded every 5 minutes while the animals were unconscious. First, phacoemulsification was performed for all three animals, and the OCE imaging was conducted for 3 times in each animal. Intra-vitreous injection of 0.3 mL sterile air was performed and then the eyes were treated with antibiotic ointment and 1% atropine immediately to prevent infection and to maintain postoperative cycloplegia. One week later, a 3-port 23-G pars plana vitrectomy (PPV) was performed with the Stellaris PC platform (Bausch & Lomb, Rochester, NY, USA) in a sterile environment. A microelectrode was then inserted through a temporal sclerotomy (approximately 4 mm in width) and was placed onto the retina below the optic nerve head (ONH) and then flattened using perfluorocarbon liquid to keep it securely attached to the retina after vitrectomy. The extraocular portion of the cable was sutured to the sclera below the conjunctiva. At the end of the procedure, the sclerotomies and conjunctiva were sutured. After the operation, topical antibiotic eye drops were used 4 times daily. And OCE imaging was performed 3 times in each animal with the implant. No complications related to surgery were observed during or after surgery.

Results

Prosthetic electrode characterization

The requirements for retinal prosthetic electrodes mainly include high electrode density, biocompatibility, and flexibility (29,30). A high-density prosthetic electrode allows high resolution stimulation and hence improves visual acuity. Due to the natural curvature of retina, flexibility enables the prosthetic electrode to adhere to the surface of the retina seamlessly for a prolonged period of time. Polyimide has the advantages of flexibility, mechanical stability, biocompatibility, and thermal stability, and was therefore used as the structural material in the prosthetic electrode. The three-dimensional platinum (Pt)-pillar coating method was used to increase the electrode density and constrain the electrode size while maintaining flexibility of the entire structure (31).

Figure 2A shows the structure of the prosthetic electrode. The multi-electrode array is connected with a high lead count cable for retinal stimulation. The array has 14×9 elements with a diameter of 150 μm each. The length of the prosthetic electrodes and the array is 37 and 3.5 mm, respectively. *Figure 2B,C,D* demonstrates the prosthetic electrode's flexibility which facilitates seamless bonding to the complex surface of the retina.

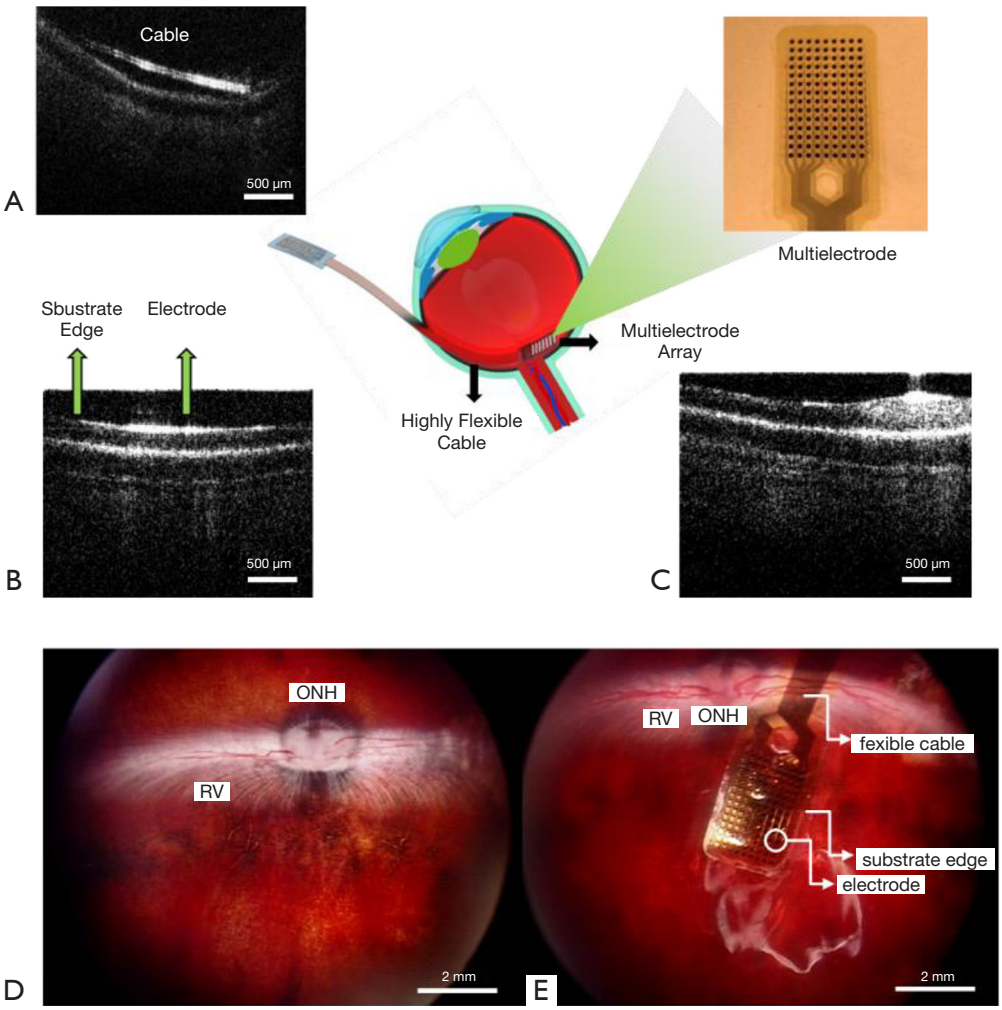

Figure 3 OCT cross-section and RetCam images of retina with prosthetic electrode. (A,B,C) Cross-sectional OCT images of retina with prosthetic electrode; (D,E) RetCam images of retina after phacoemulsification procedure and implantation procedure respectively. OCT, optical coherence tomography; ONH, optic nerve head; RV, retina vessels.

Surgery characterization

Post-surgery evaluation is essential in this study. Failure of implantation is common in phacoemulsification and implantation procedures. Hemorrhage and iris bleeding are also rarely observed during vitrectomy due to the high viscosity of vitreous humor (32,33). Retinal detachment can occur during prosthetic electrode implantation when vitreous humor is not fully removed prior to the procedure. *Figure 3* demonstrates successful implantation and bonding of the prosthetic electrode to the retina. *Figure 3A,B,C* show cross-sectional OCT images with the prosthetic electrode. *Figure 3D,E* show the *en face* RetCam (Natus Medical Incorporated, Pleasanton, CA, USA) images after phacoemulsification and implantation respectively.

Biomechanical response of retina to the prosthetic electrode

To investigate the influence of the prosthetic electrode on the retina, OCE imaging was performed after phacoemulsification and implantation. As with our previous work (25), here we segment the raw measured data to five different layers according to the anatomy of the retina and assign them respective numerals i through v for efficient classification. Layer i to layer v correspond to the nerve fiber, ganglion cell, and inner plexiform layer; inner nuclear, outer plexiform, and outer nuclear layer; retinal pigmented epithelium layer; choroid layer; choroid and sclera layer

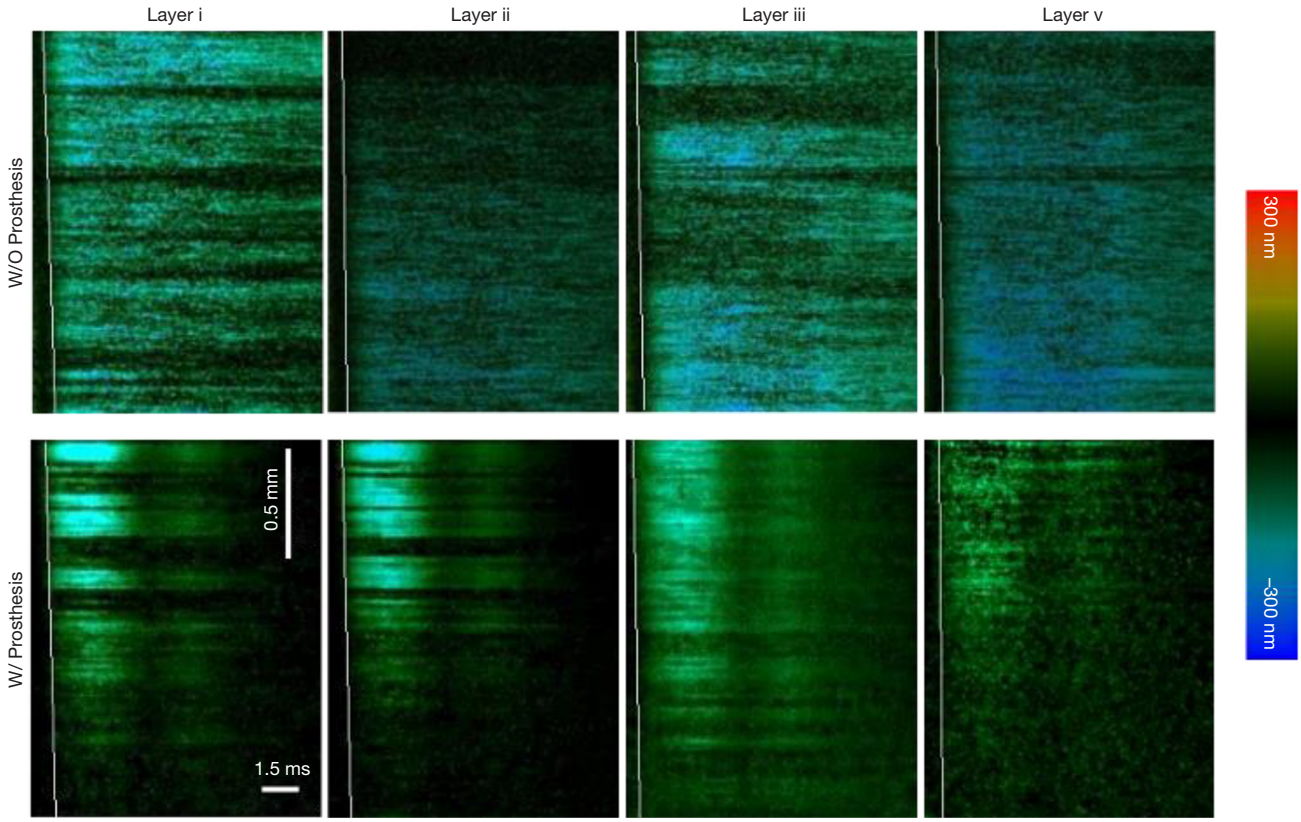

Figure 4 Spatial-temporal maps in each layer of retina with and without prosthetic electrode. The slope of the white line represents the corresponding elastic wave speed. Color bar represents the axial displacement.

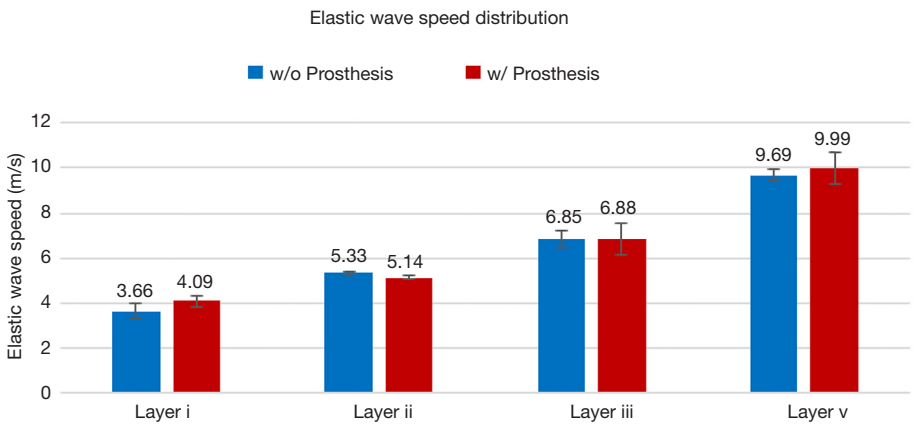

Figure 5 Statistical analysis of elastic wave speed in each layer of the retina with and without prosthetic electrode.

respectively. Spatial-temporal maps were constructed in each layer along with lateral positions and time except for layer iv due to its low OCT signal which is similar to our previously reported study (25). *Figure 4* shows the spatial-temporal map in each layer with and without the prosthetic electrode. The slope of the wavefront is the elastic wave speed in the corresponding retinal layer. *Figure 5* shows the statistical analysis of elastic wave speed in each layer with and without the prosthetic electrode; the error bar represents the standard deviation. Without the prosthetic

electrode, the elastic wave speed of layers i, ii, iii, and v is 3.66±0.36, 5.33±0.07, 6.85±0.37, and 9.69±0.24 m/s, respectively. With the prosthetic electrode, the elastic wave speed in each corresponding layer is 4.09±0.26, 5.14±0.11, 6.88±0.70, and 9.99±0.73 m/s, respectively. The difference between the results in each group and each layer were evaluated using a Shapiro-Wilk test and a paired *t*-test. The statistical analysis showed that the elastic wave speed distributes normally with $P<0.05$ in each layer of the retina. The elastic wave speed in retina with electrode was slightly higher where $P<0.05$ with an average of 2.03 m/s, and the 95% confidence interval was from 0.53 to 2.82 m/s. The elastic wave propagates faster along the depth direction of the retina, indicating the elasticity increased from the ganglion side to the photoreceptor side. The photoreceptor side is close to the sclera. The sclera is stiffer than retina, and this close-knit structure of retinal layers is likely to affect the biomechanical properties.

Discussion

In this paper, we have presented the first reported evaluation of biomechanical effects at the back of the eye in the presence of retinal prosthetic electrodes. We developed an OCE system with a mechanical shaker to induce and track elastic wave propagation in the posterior of the eye. Our highly sensitive and high spatial resolution OCE system enables detection of axial displacements precisely, which leads to high accuracy of subsequent post-processing and wave speed estimation. We used a mechanical shaker as a vibrating source to induce tissue motion. Although the shaker we used currently cannot be confocal with the OCT scanning beam, it has great practical potential for translation to clinical use compared with other vibration sources. The current tilted shaker configuration may induce complex waves instead of pure shear waves which may lead to some bias in the estimation of the wave speed. However, in previous work we showed the accuracy of our system with similar settings to those that were used here (25). The reconstructed Young's modulus of imaged phantoms was comparable to uniaxial mechanical testing with a stand-alone elasticity measurement system (Model 5942, Instron Corp., MA, USA).

Previous work to evaluate the performance of the prosthetic electrode included perceptual threshold and electrode impedance calculation, visual functions testing, and analysis of the morphology of both the retina and prosthetic electrode (7,8). The tests confirmed the safety and reliability of the prosthetic electrode but did not investigate biomechanical properties of the eye in the presence of the implanted electrode. In the current study, we investigated how the prosthetic electrode affects the biomechanical properties of the retina to help further knowledge and general understanding of these important effects.

In this study, we measured the elastic wave speed before and after prosthetic electrode implantation. Results showed that the measured biomechanical properties of the retina are comparable in each layer of tissue with and without the prosthetic electrode, and also remained consistent with biomechanics of the unaltered retina as reported in previous work (25). The prosthetic electrode is mainly composed of PI which has a density of ~1.4 g/cm^3 and is similar to the density of fluid in the posterior chamber of the eye. Furthermore, the flexibility of the lightweight prosthetic electrode allowed it to bond seamlessly to the retinal surface, thereby eliminating unwanted strain force which limited the biomechanical effects on the retina.

Although we have successfully demonstrated the effects of the prosthetic electrode on retinal biomechanical properties, there are still some challenges that can be addressed in future work. First, elastic wave speed was used for evaluating the biomechanics. Previous studies have shown that this method can induce bias estimation in thin, viscous, anisotropic, and inhomogeneous media (34-36). To solve this problem, Shih *et al.* (19) and Han *et al.* (37) implemented a Lamb Wave model using ultrasound elastography and OCE respectively to calculate the elasticity and viscosity of the cornea. The Lamb Wave model assumes the imaged target is a single thin layer, however, the retina has 5 layers, making the model inappropriate in this study. Zvietcovich *et al.* (35) developed reverberant 3D OCE to capture the elastic wave propagation in each layer of the cornea with excellent contrast. In future work, we will implement an appropriate model for biomechanical property reconstruction of the retina. Second, the quality of our OCT results is not optimal compared with OCT images of the retina in normal eyes. One important reason for this observed effect was that the eyes we used underwent phacoemulsification, vitrectomy and implantation. All of these procedures were likely to cause corneal swelling due to intraocular pressure (IOP) variation when balanced salt solution (BSS) was infused into the eye. The cornea therefore experienced excess stress and strain, which damaged the endothelium cells and led to blurring. A second important cause of reduced OCT quality in these studies is that intraocular inflammation usually occurs during vitrectomy (32,33),

resulting in intraocular blurring. Last, the metal electrode blocked the optical path of the OCT system, with the beam only able to penetrate through the gap between electrodes which led to a decrease in the OCT signal. All of these factors degraded the OCT image quality in this study. While these issues are currently difficult to resolve with our current system and setup, in future work we plan to use improved surgical techniques and a new high power OCT system to improve the image quality. This study is also limited by the lack of electrical stimulation during OCE imaging. However, the aim of this study was to explore the effects of the prosthetic electrode on the biomechanics of the retina. Further studies are needed to apply a range of electrical stimuli and investigate the corresponding biomechanical effects.

Conclusions

In summary, our work demonstrated surgical implantation of a prosthetic electrode in rabbit eye, and the biomechanical response of the retina to the prosthetic electrode. Based on the elastic wave speed from the measured data in each layer of the retina with and without the prosthetic electrode, we conclude that the prosthetic electrode does not affect the biomechanical properties of the retina significantly. We hope that this technology can be further translated into the clinical use so that it can evaluate retinal biomechanics in patients with retinal prosthetic electrodes for longitudinal study over an extended period of time.

Acknowledgments

We thank Dr. Yi Zhang for prosthetic electrode preparation, and Dr. Robert Wodnicki for proofreading.
Funding: This work was partially supported by the NIH NEI grant R01EY028662, R01EY026091, NIH P30EY029220, and an Unrestricted Departmental Grant from Research to Prevent Blindness, New York, NY 10017. ZD was a visiting scholar at Roski Eye Institute, University of Southern California.

Footnote

Provenance and Peer Review: With the arrangement by the Guest Editors and the editorial office, this article has been reviewed by external peers.

Conflicts of Interest: All authors have completed the ICMJE uniform disclosure form (available at http://dx.doi.org/10.21037/qims-20-1137). The special issue "Advanced Optical Imaging in Biomedicine" was commissioned by the editorial office without any funding or sponsorship. Dr. ZC reports personal fees from OCT Medical Imaging Inc., outside the submitted work; In addition, Dr. ZC has a patent US 16/402,591 pending. The authors have no other conflicts of interest to declare.

Ethical Statement: This study was approved by the University of Southern California Institutional Animal Care and Use Committee (IACUC).

References

1. Humayun MS, deJuan E, Dagnelie G, Greenberg RJ, Prost RH, Phillips DH. Visual perception elicited by electrical stimulation of retina in blind humans. Arch Ophthalmol 1996;114:40-6.
2. Hartong DT, Berson EL, Dryja TP. Retinitis pigmentosa. Lancet 2006;368:1795-809.
3. Jager RD, Mieler WF, Miller JW. Medical progress: Age-related macular degeneration. N Engl J Med 2008;358:2606-17.
4. Humayun MS, Weiland JD, Fujii GY, Greenberg R, Williamson R, Little J, Mech B, Cimmarusti V, Van Boemel G, Dagnelie G, de Juan E. Visual perception in a blind subject with a chronic microelectronic retinal prosthesis. Vision Res 2003;43:2573-81.
5. Luo YHL, da Cruz L. The Argus (R) II Retinal Prosthesis System. Progress in Retinal and Eye Research 2016;50:89-107.
6. Zhou DD, Dorn JD, Greenberg RJ, Grp AIS. The Argus (R) Ii Retinal Prosthesis System: An Overview. Electronic Proceedings of the 2013 Ieee International Conference on Multimedia and Expo Workshops (Icmew) 2013.
7. da Cruz L, Dorn JD, Humayun MS, Dagnelie G, Handa J, Barale PO, Sahel JA, Stanga PE, Hafezi F, Safran AB,

Salzmann J, Santos A, Birch D, Spencer R, Cideciyan AV, de Juan E, Duncan JL, Eliott D, Fawzi A, de Koo LCO, Ho AC, Brown G, Haller J, Regillo C, Del Priore LV, Arditi A, Greenberg RJ, Grp AIS. Five-Year Safety and Performance Results from the Argus II Retinal Prosthesis System Clinical Trial. Ophthalmology 2016;123:2248-54.
8. Yue L, Falabella P, Christopher P, Wuyyuru V, Dorn J, Schor P, Greenberg RJ, Weiland JD, Humayun MS. Ten-Year Follow-up of a Blind Patient Chronically Implanted with Epiretinal Prosthesis Argus I. Ophthalmology 2015;122:2545-+.
9. Stronks HC, Dagnelie G. The functional performance of the Argus II retinal prosthesis. Expert Rev Med Devices 2014;11:23-30.
10. Dagnelie G, Christopher P, Arditi A, da Cruz L, Duncan JL, Ho AC, Olmos de Koo LC, Sahel JA, Stanga PE, Thumann G, Wang Y, Arsiero M, Dorn JD, Greenberg RJ, Argus IISG. Performance of real-world functional vision tasks by blind subjects improves after implantation with the Argus (R) II retinal prosthesis system. Clin Exp Ophthalmol 2017;45:152-9.
11. Rabinowitz YS. Keratoconus. Surv Ophthalmol 1998;42:297-319.
12. Sigal IA, Flanagan JG, Ethier CR. Factors influencing optic nerve head biomechanics. Invest Ophthalmol Vis Sci 2005;46:4189-99.
13. Braunsmann C, Hammer CM, Rheinlaender J, Kruse FE, Schaffer TE, Schlotzer-Schrehardt U. Evaluation of Lamina Cribrosa and Peripapillary Sclera Stiffness in Pseudoexfoliation and Normal Eyes by Atomic Force Microscopy. Invest Ophthalmol Vis Sci 2012;53:2960-7.
14. Quigley HA. The contribution of the sclera and lamina cribrosa to the pathogenesis of glaucoma: diagnostic and treatment implications. New Trends in Basic and Clinical Research of Glaucoma: A Neurodegenerative Disease of the Visual System, Pt A 2015;220:59-86.
15. He Y, Qu Y, Zhu J, Zhang Y, Saidi A, Ma T, Zhou Q, Chen Z. Confocal Shear Wave Acoustic Radiation Force Optical Coherence Elastography for Imaging and Quantification of the In Vivo Posterior Eye. IEEE J Sel Top Quantum Electron 2019;25:10.
16. Pavlatos E, Pan XL, Clayson K, Hart RT, Weber P, Liu J. ONH Deformation in Human Eyes Using Ultrasound Speckle Tracking. Invest Ophthalmol Vis Sci 2017;58.
17. Zhou B, Chen JJ, Kazemi A, Sit AJ, Zhang X. An Ultrasound Vibro-Elastography Technique for Assessing Papilledema. Ultrasound Med Biol 2019;45:2034-9.
18. Qian X, Ma T, Yu M, Chen X, Shung KK, Zhou Q. Multi-functional Ultrasonic Micro-elastography Imaging System. Sci Rep 2017;7:1230.
19. Shih CC, Qian XJ, Ma T, Han ZL, Huang CC, Zhou QF, Shung KK. Quantitative Assessment of Thin-Layer Tissue Viscoelastic Properties Using Ultrasonic Micro-Elastography With Lamb Wave Model. IEEE Trans Med Imaging 2018;37:1887-98.
20. Qian X, Ma T, Shih CC, Heur M, Zhang J, Shung KK, Varma R, Humayun MS, Zhou Q. Ultrasonic Microelastography to Assess Biomechanical Properties of the Cornea. IEEE Trans Biomed Eng 2019;66:647-55.
21. Jin Z, Khazaeinezhad R, Zhu J, Yu JX, Qu YQ, He YM, Li Y, Alvarez-Arenas TEG, Lu F, Chen ZP. In-vivo 3D corneal elasticity using air-coupled ultrasound optical coherence elastography. Biomed Opt Express 2019;10:6272-85.
22. Li Y, Moon S, Chen JJ, Zhu Z, Chen Z. Ultrahigh-sensitive optical coherence elastography. Light Sci Appl 2020;9:58.
23. Qu Y, Ma T, He Y, Zhu J, Dai C, Yu M, Huang S, Lu F, Shung KK, Zhou Q, Chen Z. Acoustic Radiation Force Optical Coherence Elastography of Corneal Tissue. IEEE J Sel Top Quantum Electron 2016;22:6803507.
24. Li Y, Zhu J, Chen JJ, Yu JX, Jin Z, Miao YS, Browne AW, Zhou QF, Chen ZP. Simultaneously imaging and quantifying in vivo mechanical properties of crystalline lens and cornea using optical coherence elastography with acoustic radiation force excitation. APL Photonics 2019;4:106104.
25. Qian X, Li R, Li Y, Lu G, He Y, Humayun MS, Chen Z, Zhou Q. In vivo evaluation of posterior eye elasticity using shaker-based optical coherence elastography. Exp Biol Med (Maywood) 2020;245:282-8.
26. Du Z, Li R, Qian X, Lu G, Li Y, He Y, Qu Y, Jiang L, Chen Z, Humayun MS, Chen Z, Zhou Q. Quantitative confocal optical coherence elastography for evaluating biomechanics of optic nerve head using Lamb wave model. Neurophotonics 2019;6:041112.
27. Wang S, Li JS, Manapuram RK, Menodiado FM, Ingram DR, Twa MD, Lazar AJ, Lev DC, Pollock RE, Larin KV. Noncontact measurement of elasticity for the detection of soft-tissue tumors using phase-sensitive optical coherence tomography combined with a focused air-puff system. Opt Lett 2012;37:5184-6.
28. Ambroziński Ł, Song SZ, Yoon SJ, Pelivanov I, Li D, Gao L, Shen TT, Wang RKK, O'Donnell M. Acoustic micro-tapping for non-contact 4D imaging of tissue elasticity. Sci Rep 2016;6:38967.

29. Rodger DC, Weiland JD, Humayun MS, Tai YC. Scalable high lead-count parylene package for retinal prostheses. Sensors and Actuators B-Chemical 2006;117:107-14.
30. Zeng Q, Zhao SS, Yang HG, Zhang Y, Wu TZ. Micro/Nano Technologies for High-Density Retinal Implant. Micromachines (Basel) 2019;10:419.
31. Xia K, Sun B, Zeng Q, Wu TZ, Humayun MS. Surface Modification of Neural Stimulating/Recording Microelectrodes with High-Performance Platinum-Pillar Coatings. 2017 Ieee 12th International Conference on Nano/Micro Engineered and Molecular Systems (Nems) 2017:291-4.
32. Park SS, Marcus DM, Duker JS, Pesavento RD, Topping TM, Frederick AR, Damico DJ. Posterior Segment Complications after Vitrectomy for Macular Hole. Ophthalmology 1995;102:775-81.
33. Gupta OP, Weichel ED, Regillo CD, Fineman MS, Kaiser RS, Ho AC, McNamara JA, Vander JF. Postoperative complications associated with 25-gauge pars plana vitrectomy. Ophthalmic Surg Lasers Imaging 2007;38:270-5.
34. Kirby MA, Pelivanov I, Song SZ, Ambrozinski L, Yoon SJ, Gao L, Li D, Shen TT, Wang RK, O'Donnell M. Optical coherence elastography in ophthalmology. J Biomed Opt 2017;22:1-28.
35. Zvietcovich F, Pongchalee P, Meemon P, Rolland JP, Parker KJ. Reverberant 3D optical coherence elastography maps the elasticity of individual corneal layers. Nat Commun 2019;10:4895.
36. Parker KJ, Ormachea J, Zvietcovich F, Castaneda B. Reverberant shear wave fields and estimation of tissue properties. Phys Med Biol 2017;62:1046-61.
37. Han Z, Aglyamov SR, Li J, Singh M, Wang S, Vantipalli S, Wu C, Liu CH, Twa MD, Larin KV. Quantitative assessment of corneal viscoelasticity using optical coherence elastography and a modified Rayleigh-Lamb equation. J Biomed Opt 2015;20:20501.

Cite this article as: Li R, Du Z, Qian X, Li Y, Martinez-Camarillo JC, Jiang L, Humayun MS, Chen Z, Zhou Q. High resolution optical coherence elastography of retina under prosthetic electrode. Quant Imaging Med Surg 2021;11(3):918-927. doi: 10.21037/qims-20-1137

